NON-REDUNDANT, LINEAR-PHASE, SEMI-ORTHOGONAL, DIRECTIONAL COMPLEX WAVELETS

Felix C. A. Fernandes,[t] *Michael B. Wakin*[r] *and Richard G. Baraniuk*[r]

[t] DSPS R&D Center, Texas Instruments, Dallas TX, USA
[r] Department of Electrical and Computer Engineering, Rice University, Houston TX, USA

ABSTRACT

The directionality and phase information provided by non-redundant complex wavelet transforms (NCWTs) provide significant potential benefits for image/video processing and compression applications. However, because existing NCWTs are created by downsampling filtered wavelet coefficients, the finest scale of these transforms has resolution $4\times$ lower than the real input signal. In this paper, we propose a linear-phase, semi-orthogonal, directional NCWT design using a novel *triband* filter bank. At the finest scale, the resulting transform has resolution $3\times$ lower than the real input signal. We provide a design example to demonstrate three important properties for image/video processing applications: directionality, magnitude coherency, and phase coherency.

1. INTRODUCTION

Complex wavelet transforms, in which the real and imaginary parts of the transform coefficients are an approximate Hilbert-transform pair [1, 2], offer three significant advantages over real wavelet transforms: shift invariance, directionality, and explicit phase information. These properties enable efficient statistical models for the coefficients that are also *geometrically* meaningful. In [3], for example, we identify distinct relationships between complex coefficient magnitudes and phases, and edge orientations and positions, respectively. Using these relationships, we develop an effective Geometric Hidden Markov Tree (GHMT) model for the complex wavelet coefficients.

Unfortunately, the success of geometric modeling in complex wavelet coefficients has been limited to the class of *redundant*, or overcomplete, complex transforms. This redundancy complicates any application to problems such as image/video compression where parsimonious signal representations are critical. To address this issue, some researchers [4–6] have devised Non-Redundant Complex Wavelet Transforms (NCWTs). Each of these implementations can be viewed as a combination of a downsampled positive-frequency projection filter with a traditional dual-band real wavelet transform. Therefore, at the finest scale, the complex wavelet transform has resolution $4\times$ lower than the real input signal. These NCWTs do enjoy directionality and explicit phase information because of the approximate Hilbert-transform relationship between real and imaginary parts of their transform coefficients. To date, however, they have been significantly less amenable to geometric modeling than their redundant counterparts.

In this paper, we propose a linear-phase, semi-orthogonal, directional NCWT design using a novel *triband* (downsample by 3) filter bank (see Fig. 1). As we explain, a triband approach permits a natural, direct NCWT implementation using complex wavelet filters and a real scaling filter. At the finest scale, the resulting complex wavelet transform has resolution $3\times$ lower than the real input signal. We provide a design example and illustrate some properties that may make our 2D non-redundant coefficients amenable to geometric modeling.

This work was supported by the Texas Instruments Leadership University Program, NSF, ONR, AFOSR, and DARPA. Email: felixf@ti.com, {wakin,richb}@rice.edu. Web: dsp.rice.edu.

2. A NON-REDUNDANT CWT

We now demonstrate how to construct a novel 2D NCWT as a separable extension of two 1D triband NCWTs that we label NCWT*R* and NCWT*C*. The 1D NCWT*R* (Fig. 2) operates on *R*eal inputs while the 1D NCWT*C* (Fig. 3) operates on *C*omplex inputs. The idealized magnitude responses for the NCWT*R* and NCWT*C* filters are depicted in Fig. 1. Consider the block diagram in Fig. 4. The notation $X(z_1, z_2)$ denotes the z-transform of a real-valued digital image $x(n_1, n_2)$. To perform the 2D NCWT, first apply the 1D NCWT*R* on the rows of $X(z_1, z_2)$ to obtain a real-valued, lowpass subband $X_0(z_1, z_2)$ and a complex-valued, highpass subband $X_+(z_1, z_2)$. The frequency-domain support of these subbands is depicted in Fig. 5. In Section 2.2, we shall explain that redundancy considerations justify the elimination of the subband $X_-(z_1, z_2)$ because $X_-(z_1, z_2)$ is the complex conjugate of $X_+(z_1, z_2)$ for real-valued input, $X(z_1, z_2)$. We complete the 2D NCWT by performing two different 1D transforms along the columns of the subbands $X_0(z_1, z_2)$ and $X_+(z_1, z_2)$. Because the subband $X_0(z_1, z_2)$ contains real-valued transform coefficients, we apply the 1D NCWT*R* to the subband columns, thereby obtaining two output subbands $X_{00}(z_1, z_2)$ and $X_{0+}(z_1, z_2)$. (Once again, the subband $X_{0-}(z_1, z_2)$ is discarded because it is redundant.) Finally, we apply the 1D NCWT*C* to the complex coefficients of the $X_+(z_1, z_2)$ subband to obtain three output subbands $X_{+0}(z_1, z_2)$, $X_{++}(z_1, z_2)$ and $X_{+-}(z_1, z_2)$.

The first level of the 2D NCWT is now complete. The five output subbands partition the frequency domain as shown in Fig. 6. This transform has higher directionality than the real wavelet transform, because the latter transform cannot differentiate between features oriented at 45 and -45 degrees. Subsequent levels of the transform are obtained by recursively transforming the lowpass subband $X_{00}(z_1, z_2)$. The 2D NCWT is easily inverted by apply-

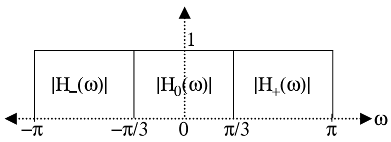

Fig. 1. *Idealized magnitude responses of triband filters.*

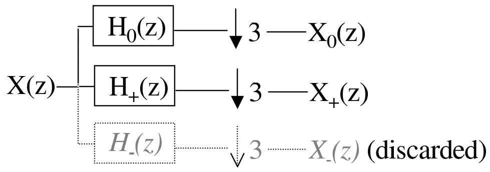

Fig. 2. *1D NCWTR for real signals.*

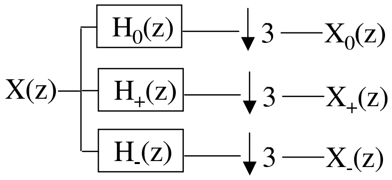

Fig. 3. *1D NCWTC for complex-valued signals.*

ing the appropriate 1D synthesis filter banks along the columns and rows of the 2D transform coefficients. In the following subsections, we shall design the 1D NCWT*C* and 1D NCWT*R*.

2.1. 1D NCWT*C* for Complex-Valued Signals

Fig. 3 shows the 3-band analysis filter bank that performs the first level of a non-redundant complex wavelet decomposition of $X(z)$, the z-transform of $x(n)$, a complex-valued input signal. $H_0(z)$ has real filter coefficients while $H_+(z)$ and $H_-(z)$ have complex filter coefficients such that $H_+^*(z) = H_-(z)$, which signifies that the $H_+(z)$ filter coefficients are complex conjugates of the $H_-(z)$ filter coefficients. The idealized magnitude responses of these filters are shown in Fig. 1. Provided that $H_0(z)$ satisfies existence conditions [7], $X_0(z)$ represents a scaling-coefficient sequence while $X_+(z)$ and $X_-(z)$ represent wavelet-coefficient sequences. Because $|H_+(\omega)|$ and $|H_-(\omega)|$ have one-sided magnitude responses in Fig. 1, each of the wavelet coefficient sequences $X_+(z)$ and $X_-(z)$ exhibits a Hilbert-transform relationship between their real and imaginary parts. This property will enable directionality and explicit phase information in the 2D NCWT. The following argument shows that the decomposition provided by Fig. 3 is non-redundant. Let the input signal $x(n)$ consist of N complex numbers. Then due to the decimation in each subband, the subband signals $x_0(n), x_+(n), x_-(n)$ each have $N/3$ complex coefficients. Since the input and the transform coefficients each require the same amount of storage space (for N complex numbers), the transform is non-redundant.

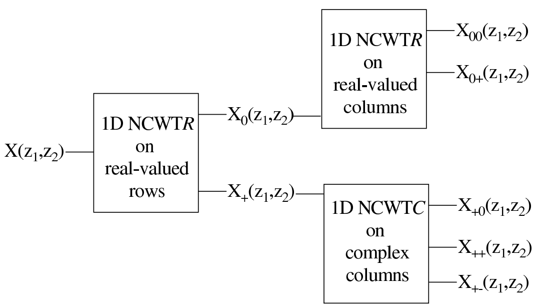

Fig. 4. *Implementation of the 2D NCWT.*

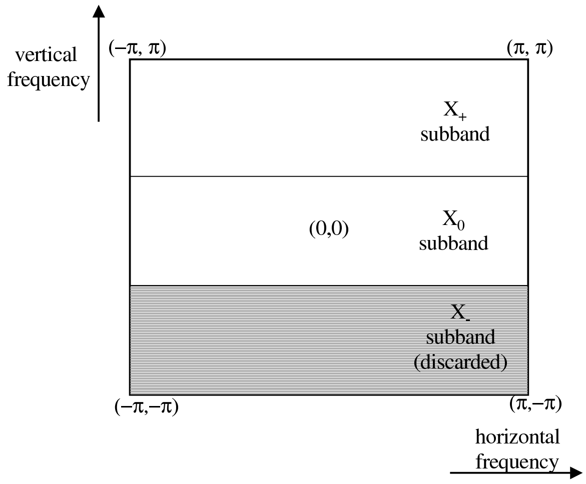

Fig. 5. *Frequency-domain partitioning after 1D NCWTR on image rows.*

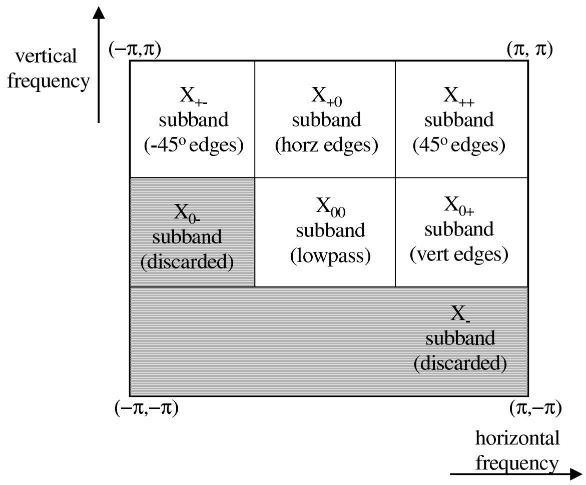

Fig. 6. *Frequency-domain partitioning after 2D NCWT.*

To implement the analysis filter bank in Fig. 3, we must address the following design issues.

1. The frequency responses of the analysis filters must approximate the idealized magnitude responses in Fig. 1.
2. To ensure that the 1D NCWT*R* in Section 2.2 is non-redundant, we must have $H_+^*(z) = H_-(z)$.
3. To obtain smooth basis functions, $H_0(z)$ must satisfy existence and vanishing-moment conditions [7].
4. For image/video compression applications, the $H_0(z)$, $H_+(z)$, $H_-(z)$ filter bank should be linear-phase and orthogonal [7].
5. A synthesis filter bank that reconstructs $X(z)$ from the subband signals $X_0(z), X_+(z), X_-(z)$ must exist [7].

Multi-band filter bank design is a difficult problem, and no direct design method satisfies all the above criteria simultaneously. Therefore, we have adopted the following approach to design our analysis filter bank. First, we use Tran *et al.*'s parameterization

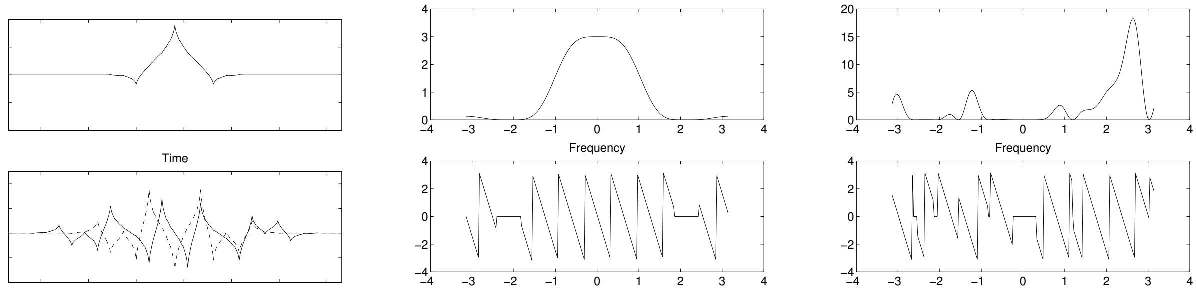

(a) (b) (c)

Fig. 7. *(a) Top: scaling function associated with $H_0(z)$. Bottom: complex wavelet associated with $H_+(z)$ (real part solid; imaginary part dashed). (b) Magnitude and phase response of $H_0(z)$. (c) Magnitude and phase response of $H_+(z)$.*

[8] to specify a length-9, 3-band, orthogonal, linear-phase, real-coefficient filter bank. We then exploit the free parameters to impose two vanishing moments on the scaling filter. In the resulting system, let $\widehat{E}(z)$ denote the polyphase matrix [7] of the analysis filter bank. Define

$$C = \begin{bmatrix} 1 & 0 & 0 \\ 0 & \frac{1}{\sqrt{2}} & \frac{j}{\sqrt{2}} \\ 0 & \frac{1}{\sqrt{2}} & \frac{-j}{\sqrt{2}} \end{bmatrix}, \; S = \begin{bmatrix} 1 & 0 & 0 \\ 0 & \cos(\theta) & \sin(\theta) \\ 0 & -\sin(\theta) & \cos(\theta) \end{bmatrix}.$$

Now, the first, second and third rows of the polyphase matrix $C\widehat{E}(z)$ contain the polyphase components for $H_0(z), H_+(z)$ and $H_-(z)$ respectively. These analysis filters satisfy all preceding constraints except for Constraint 1, which is violated because the magnitude responses $|H_+(\omega)|, |H_-(\omega)|$ differ from the idealized responses in Fig. 1. To satisfy Constraint 1, we must improve the wavelet-filter magnitude responses by introducing free optimization parameters without violating the other constraints. Therefore, we define

$$U(z) = \begin{bmatrix} z^{-1} & 0 & 0 \\ 0 & z^{-1} & u - uz^{-2} \\ 0 & 0 & z^{-1} \end{bmatrix},$$

$$V(z) = \begin{bmatrix} z^{-1} & 0 & 0 \\ 0 & z^{-1} & 0 \\ 0 & v - vz^{-2} & z^{-1} \end{bmatrix}$$

and generate a new analysis filter bank with polyphase matrix $E(z)$ defined by $E(z) = CV(z)U(z)S\widehat{E}(z)$. Observe that the entries in the first rows of $C, S, U(z), V(z)$ guarantee that the scaling filter specified by $E(z)$ is the same (modulo shifts) as the scaling filter specified by $\widehat{E}(z)$. Hence Constraint 3 is still satisfied by the $E(z)$ system. Now, S introduces the free parameter θ into $E(z)$ without affecting Constraint 4 because S is orthogonal and also preserves linear phase. Next, consider the matrices $U(z), V(z)$. These are left-extension matrices [9] that lengthen the wavelet filters by introducing free parameters u, v into the analysis filter bank while preserving linear phase. However, orthogonality of the wavelet filters is not preserved by these matrices. The zeros in the first rows and first columns of the left-extension matrices ensure that the the scaling filter specified by $V(z)U(z)S\widehat{E}(z)$ is orthogonal to its own shifts as well as to shifts of the wavelet filters, although the wavelet filters are not orthogonal to their own shifts. Thus, in addition to semi-orthogonality [7], the basis associated with the $V(z)U(z)S\widehat{E}(z)$ system also has orthogonal scaling functions. Therefore, the $V(z)U(z)S\widehat{E}(z)$ filter bank satisfies a weakened form of Constraint 4 in which "orthogonal" is replaced by "semi-orthogonal and $H_0(z)$ should be shift-orthogonal." Note that the scaling filter and two wavelet filters associated with the $V(z)U(z)S\widehat{E}(z)$ system have lengths 9, 15, 21 respectively, because the $U(z)$ and $V(z)$ lengthen the original length-9 $\widehat{E}(z)$ system. Finally, the matrix C is introduced to transform the real-coefficient polyphase matrix $V(z)U(z)S\widehat{E}(z)$ into $E(z)$, the second and third rows of which specify complex-coefficient filters $H_+(z)$ and $H_-(z)$ that satisfy Constraint 2. By optimizing over the real-valued, free parameters θ, u, v, we obtained $E(z)$ with wavelet-filter magnitude responses that have minimum mean-squared error with respect to the idealized responses in Fig. 1. With ^{H} representing the Hermitian transpose, the polyphase matrix for the synthesis filter bank corresponding to $E(z)$ is given by $R(z) = \widehat{E}^H(z^{-1})S^H U(z^{-1})V(z^{-1})C^H$ because $\widehat{E}^H(z), S, C$ are paraunitary and $U(z)^{-1} = U(z^{-1}), V(z)^{-1} = V(z^{-1})$. In Fig. 7(a), we depict the scaling function associated with $H_0(z)$ and the complex wavelet associated with $H_+(z)$, while in Fig. 7(b) and Fig. 7(c), we show the frequency responses for $H_0(z)$ and $H_+(z)$, respectively.

2.2. 1D NCWT*R* for Real-Valued Signals

Creating the 1D NCWT*R* necessitates slight modifications to the filter banks of the previous section. Consider Fig. 3 and assume that the input $x(n)$ is a real-valued signal consisting of N real numbers. Since $H_0(z)$ has real coefficients, $x_0(n)$ has $N/3$ real numbers, while $x_+(n)$ and $x_-(n)$ each have $N/3$ complex numbers. However, because complex numbers have real and imaginary parts, the transform coefficients $x_0(n), x_+(n), x_-(n)$ require storage space for $5N/3$ real numbers. Therefore, for real-valued input, this transform is redundant because the transform coefficients require more storage space than the input signal.

To obtain a non-redundant transform for real-valued input, observe that $x_-(n)$ is the complex conjugate of $x_+(n)$, because $x(n)$ is real-valued and $H_+^*(z) = H_-(z)$. Therefore $x_-(n)$ contains the same information as $x_+(n)$, and may be discarded because it is redundant. Fig. 2 shows the modified analysis filter bank for the 1D NCWT*R* after eliminating the $H_-(z)$ branch in Fig. 3. In this case, if $x(n)$ has N real numbers, then $x_0(n)$ and $x_+(n)$ have $N/3$ real numbers and $N/3$ complex numbers respectively. The transform is now non-redundant because the input signal and transform coefficients each require the same amount of storage space. To reconstruct $X(z)$, we can generate $X_-(z)$ from $X_+(z)$ by setting

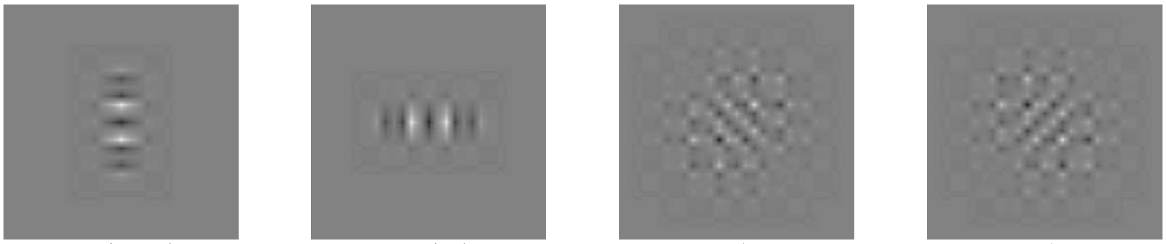

Horizontal Vertical $+45$ -45

Fig. 8. *2D complex wavelet basis functions (imaginary parts shown).*

Fig. 9. *Left:* Barbara *image. Center and right: magnitudes and phases of vertical subband complex wavelet coefficients.*

$X_-(z) = X_+^*(z)$ and then using the synthesis filter bank associated with the 1D NCWT*C* in Section 2.1. In practice, we actually reconstruct $X(z)$ without generating $X_-(z)$. Instead, we use $X_0(z)$ and the real and imaginary parts of $x_+(n)$ as input to the synthesis polyphase matrix $\widehat{E}^H(z^{-1})S^H U(z^{-1})V(z^{-1})$. Due to space limitations, we omit the proof for this second reconstruction technique.

3. PROPERTIES OF THE NEW 2D TRANSFORM

In conclusion, we briefly mention some favorable 2D-NCWT properties that may be useful for image/video processing.

Directionality: Fig. 8 shows the 2D complex basis functions for the four directional wavelet subbands. As discussed in Section 2, the 2D NCWT has higher directionality than the real wavelet transform. Specifically, the filters provide distinct basis functions for the 45 and -45 degree subbands, in addition to vertical and horizontal basis functions.

Magnitude coherence: Fig. 9 shows the first-level vertical subband of the 2D NCWT of the *Barbara* image. The magnitudes successfully identify image regions with strong directional tendency. In addition (and unlike real wavelet coefficients), the magnitudes have a smooth envelope along edges.

Phase coherence: Also shown in Fig. 9 are the phases of the complex coefficients. In regions with strong directional tendency (i.e. where coefficient magnitudes are large), the phases typically demonstrate a degree of structure, or coherency.

The above properties suggest that the 2D-NCWT may be well-suited to image processing and geometric modeling. For example, a zerotree compression algorithm [10] could be developed based on coefficient magnitudes. In the future, we plan to investigate extending the GHMT [3] to the new transform. Such techniques will require a novel *nona-tree* structure due to the triband filter bank. Each complex coefficient will have 9 children (instead of 4, as with dual-band real wavelet transforms). In addition, the higher decimation provides greater frequency separation between wavelet scales (more than one octave), and so less depth will be needed in the tree.

4. REFERENCES

[1] N. Kingsbury, "Complex wavelets for shift invariant analysis and filtering of signals," *ACHA*, June 2000.

[2] P.-L. Shui, Z. Bao, and Y. Y. Tang, "Three-band biorthogonal interpolating complex wavelets with stopband suppression via lifting scheme," *IEEE Trans. Signal Proc.*, May 2003.

[3] J. K. Romberg, M. B. Wakin, H. Choi, and R. G. Baraniuk, "A geometric hidden Markov tree wavelet model," in *SPIE Wavelets X*, 2003.

[4] F. C. A. Fernandes, R. L. C. van Spaendonck, and C. S. Burrus, "A new framework for complex wavelet transforms," *IEEE Trans. Signal Proc.*, July 2003.

[5] R. van Spaendonck, T. Blu, R. Baraniuk, and M. Vetterli, "Orthogonal Hilbert transform filter banks and wavelets," in *ICASSP*, 2003.

[6] M. T. Orchard and H. Ates, "Equiripple design of real and complex filter banks," Tech. Rep., Rice University, 2003.

[7] G. Strang and T. Nguyen, *Wavelets and Filter Banks*, Wellesley-Cambridge Press, Wellesley, MA, 1996.

[8] T. D. Tran, R. L. de Queiroz, and T. Q. Nguyen, "Linear-phase perfect reconstruction filter bank: Lattice structure, design, and application in image coding," *IEEE Trans. Signal Proc.*, Jan. 2000.

[9] I. A. Shah and T. A. C. M. Kalker, "On ladder structures and linear phase conditions for bi-orthogonal filter banks," in *ICASSP*, 1994.

[10] J. M. Shapiro, "Embedded image coding using zerotrees of wavelet coefficients," *IEEE Trans. Signal Proc.*, Dec. 1993.